The impact of melt retention time on the strontium modification efficiency

Kozina, Franjo; Zovko Brodarac, Zdenka; Tubić Bulat, Barbara

Source / Izvornik: **CONFERENCE PROCEEDINGS MECHANICAL TECHNOLOGIES AND STRUCTURAL MATERIALS, 2021, 69 - 73**

Conference paper / Rad u zborniku

Publication status / Verzija rada: **Published version / Objavljena verzija rada (izdavačev PDF)**

Permanent link / Trajna poveznica: https://urn.nsk.hr/urn:nbn:hr:115:110920

Rights / Prava: In copyright/Zaštićeno autorskim pravom.

Download date / Datum preuzimanja: **2025-03-19**

Repository / Repozitorij:

Repository of Faculty of Metallurgy University of Zagreb - Repository of Faculty of Metallurgy University of Zagreb

The impact of melt retention time on the strontium modification efficiency

Franjo Kozina[1], **Zdenka Zovko Brodarac**[1], **Barbara Tubić Bulat**[1], **Franjo Dominković** [2]

1) University of Zagreb Faculty of Metallurgy
   Aleja narodnih heroja 3, 44 000 Sisak,
   Croatia

2) Proizvodnja OSO d.o.o.
   Vukomerička 9, 10410 Velika Gorica,
   Croatia

fkozin@uizg.simet.hr
zovko@unizg.simet.hr
tubicb@unizg.simet.hr
franjo.dominkovic@dalekovod.hr

Keywords

AlSi12 alloy
Strontium
Eutectic modification
Modification efficiency

Original scientific article

Abstract: The modification of eutectic (α_{Al}+β_{Si}) phase is frequently performed during processing of aluminum-silicone (Al-Si) based foundry alloys leading to a structural transformation of the eutectic β_{Si} phase from a course plate to a fine fibrous morphology. The morphological refinement of the brittle eutectic β_{Si} phase improves ductility, tensile strength, and elongation. This research was performed to estimate the influence of melt retention time on strontium (Sr) modification efficiency. For this purpose, the AlSi12 alloy with eutectic composition was produced and processed by the addition of AlSr10 master alloy. The samples for chemical, mechanical and microstructure analysis were taken with melt retention time of 20 min, 40 min and 80 min. The results of chemical composition analysis indicated the decrease in Sr content with the increase in melt retention time. The poor Sr recovery was a result of the subsequent addition of chemical degassing agents led to the gas entrapment in the melt. Consequently, the highest gas index and most severe porosities were found in sample with retention time of 20 min. The fully modified eutectic (α_{Al}+β_{Si}) phase morphology was only obtained in sample with retention time of 20 min. After melt retention time of 40 min the unmodified plate-like eutectic β_{Si} phase particles were found. Additional prolongation of melt retention time to 80 min led to the coarsening of eutectic β_{Si} phase particle. The plate-like eutectic β_{Si} phase particles were located near the primary α_{Al} dendritic network and surrounding the primary β_{Si} phase particles. This phase distribution suggests that the transformation of the primary α_{Al} dendritic network is followed by solidification of unmodified eutectic β_{Si} phase particles.

1. Introduction

The modification of eutectic (α_{Al}+β_{Si}) is frequently performed during processing of aluminum-silicone (Al-Si) based foundry alloys [1]. The modification leads to a structural transformation of the eutectic β_{Si} phase from a course plate to a fine fibrous morphology [2]. The morphological refinement of the brittle eutectic β_{Si} phase improves mechanical properties, especially ductility, tensile strength, and elongation [3]. The modification of eutectic (α_{Al}+β_{Si}) can be performed chemically, by high cooling rate, electromagnetic stirring, and ultrasonic vibration [4]. The ultrasonic melt processing is an effective method of grain and intermetallic phase refinement through the mechanisms of fragmentation and nucleation. The fragmentation of primary solidified intermetallic phases allows for the heterogeneous nucleation of α_{Al} solid solution and eutectic (α_{Al}+β_{Si}) phase [5]. The magnetic stirring enables cast microstructure refinement by promoting dendritic fragmentation ahead of the solidification front. The increased liquid convection can result in either bending of dendritic branches or dendritic root remelting [6]. In the hypereutectic Al-Si alloys the electromagnetic stirring enables refinement of the primary β_{Si} particles through cavitation effect [7]. At the cooling rates higher

than 400 μms^{-1} the solidification of the eutectic β_{Si} phase transitions from faceted to non-faceted, followed by the decrease in undercooling and twin density [8]. The chemical modification of eutectic (α_{Al}+β_{Si}) phase is based on the addition of microstructure modifying elements that can affect eutectic β_{Si} phase nucleation and growth [9]. Although, chemical modification can be performed by adding alkaline, alkaline earth and rare earth metals, phosphorus (P), sodium (Na) and strontium (Sr) are most frequently used in foundry practice [4].

The nucleation of eutectic β_{Si} phase is affected by poisoning of aluminum phosphide (AlP) particles necessary for the heterogeneous nucleation. Since poisoned Na_2P, Sr_3P_2 and Al_2Si_2Sr particles solidify prior to the eutectic reaction [4], the reduced number of heterogeneous nucleation sites forces the eutectic transformation to higher undercooling and reduces the number of eutectic grains [10].

The two most established restricted growth theories for eutectic (α_{Al}+β_{Si}) modification are the impurity-induced twining (IIT) and the twin plane re-entrant edge (TPRE) mechanism. The IIT mechanism is based on the modifier adsorption at the growth surfaces of eutectic β_{Si} phase facilitating the formation of new twins and enabling growth in many different directions [11]. The TPRE

modification mechanism proposes that the modifier retards eutectic β_{Si} phase growth by being selectively adsorbed at the growth surfaces. Consequently, modified eutectic β_{Si} phase grows isotropic in different directions. Due to the increased branching of eutectic β_{Si} phase, the decrease in undercooling is expected [12]. The level of undercooling influences both nucleation and growth of microstructure constituents during solidification process However, since the undercooling occurs in the melt before eutectic reaction starts and modification begins, the higher undercooling can occur due to the Na and Sr poisoning effect [13].

The chemical modification using P is a commonly used methods for modification of primary β_{Si} phase in hypereutectic Al-Si foundry alloys. The P, added in form of phosphorus salt, phosphorus copper master alloy or aluminum phosphorus master alloy, reacts with Al to form AlP particles with high melting point. The similarity in crystal structure between AlP particles and primary β_{Si} phase enables its heterogeneous nucleation and structure refinement [14]. The Na is added to a melt in the elemental form or as a salt at the lowest practical temperature. With the drop in melt temperature a large amount of highly dispersed sodium silicate (NaSi) particles is formed. The NaSi particles are adsorbed on the eutectic ($\alpha_{Al}+\beta_{Si}$) nucleation sites retarding the grain growth. In the Al-Si alloys with eutectic composition, Na additions increase undercooling and promote primary α_{Al} dendritic network transformation [15]. Due to the high vapor pressure, Na has a short modification period with poor and unpredictable recovery (10 – 50 % of the addition [16]) [17]. The modification using Sr is mainly performed due to its higher retention time and lack of overmodification issue [18]. Compared to Na, Sr is usually added as master alloy exhibiting more complex dissolution characteristics with better recovery (80 – 90 % of the addition [16]). Dissolution of Sr in the melt strongly depends on its content in the master alloy. Master alloys with high Sr content are added at the lowest practical temperature, while master alloys with lower Sr content give better recovery at the higher temperatures. To achieve satisfactory modification effect 0.2 – 0.5 g/kg of Sr is added to the melt [16]. Due to its high tendency towards hydrogen (H_2), the Sr is never added to the melt in combination with chemical degassing agents. Their interaction reduces the absorption of Sr into the melt, hydrogen trapping and appearance of gas porosities in the castings. The Sr modification is based on the TPRE mechanism comprehending its adsorption at the growth surfaces of eutectic β_{Si} phase and increased branching [17].

The goal of the research is to estimate the influence of melt retention time on the Sr modification efficiency during processing and casting of AlSi12 alloy. The efficiency of Sr modification was estimated by chemical composition, mechanical properties, and metallographic analysis.

2. Experimental work

In order to estimate the efficiency of Sr modification the AlSi12 alloy was produced. The input materials used in melt production and processing are given in Table 1.

The production of the melt began by remelting 80 kg of the AlSi12 master alloy with the addition of 0.8 kg Coveral 1 fluxer. The chemical composition was mended through the additions of 0.32 kg AlMn75, 0.4 kg, AlTi10 and 2.4 kg AlSi50 master alloys.

Table 2.   The input materials used in AlSi12 alloy production and processing

Input material		Amount, kg
Master alloy	AlSi12	80
	AlMn75	0.32
	AlTi10	0.4
	AlSi50	2.4
Fluxes	Coveral 1%	0.8
Microstructure modifiers	AlTi5B1	0.22
	AlSr10	0.23

The grain refinement was performed by adding 0.22 kg of AlTi5B1 master alloy. The AlSr10 master alloy was added to the melt at the temperature of 780°C before stirring with argon (Ar). After chemical modification the melt was transported into a holding furnace with constant temperature and chemical degassed. The casting process was delayed for 20 min after modification. The melt was cast into a permanent steel mold at the pouring temperature of 720±20 °C.

During the solidification in a permanent steel mold Simple Thermal Analysis (STA) was performed using temperature measuring device "National Instruments" NI-9211 with NI cDAQ-9172 thermo-module and LabVIEW Full Development System software support. The obtained cooling curves were used to identify the following characteristic temperatures: minimum liquidus temperature (T_{Lmin}), maximum liquidus temperature (T_{Lmax}), minimum eutectic temperature (T_{Emin}), maximum eutectic temperature (T_{Emax}) and solidus temperature (T_S). The obtained characteristic temperatures enabled calculation of changes in liquid (ΔT_L) and eutectic (ΔT_E) temperature as well as estimation of temperature (ΔT_{L-S}) and time (Δt_{L-S}) solidification interval.

The samples for the chemical composition analysis, density measurements, mechanical properties determination and microstructure analysis were taken 20 min (sample 1), 40 min (sample 2) and 80 min (sample 3) after the addition of Sr.

The chemical composition was analyzed using SPECTRO MAX x LMM 04 spectrometer.

Based on the Archimedes' law density values for the samples solidifying on air and under vacuum were calculated. Comparison of the calculated density values enabled determination of gas index.

The use of Radiographic measurements enabled determination of discontinuities in the clamp castings. The Radiographic measurement were performed according to the ASTM E 155-05 on the YXLON MU 2000 device.

The samples for metallographic analysis were prepared using standard grinding and polishing techniques. The samples for light microscopy were etched using 0.5 aqueous fluoric acid solution (0.5HF). The Olympus GX51 inverted metallographic microscope was used to perform light microscopy.

The tensile strength was determined using Zwick tensile testing machine. The castings were loaded under a constant speed of 5 mm/min.

3. Results

The results of chemical composition analysis are given in Table 2. The chemical composition of the produced alloy is in accordance with EN AB 44100. The amount of Si present in all three samples (Table 2) corresponds to the eutectic composition indicating solidification of eutectic ($\alpha_{Al}+\beta_{Si}$) phase. The amount of Sr is highest in the sample 1 (0.0069 wt.%). After retention time of 40 min, content of Sr drops to 0.0056 wt.%. The lowest amount of Sr was measured in sample 3 obtained after 80 min of retention time (Table 2). Based on the amount of Sr in all three samples a complete modification of eutectic ($\alpha_{Al}+\beta_{Si}$) structure is not expected (Table 2).

The cooling curve recorded at the beginning of the casting is given in Figure 1 with characteristic temperatures indicated in Table 3.

Table 2. The results of chemical composition analysis

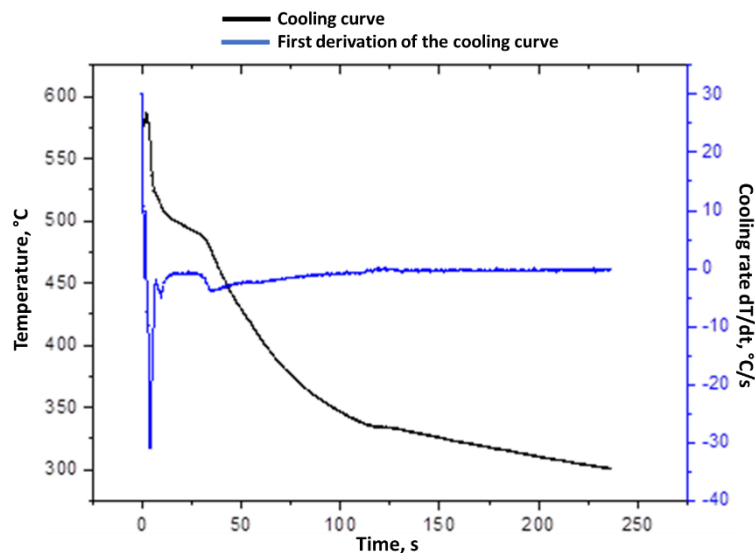| Sample	Chemical composition, wt. %									
	Si	Fe	Cu	Mn	Mg	Ni	Ti	Na	Sr	Al
1	12.190	0.112	0.0016	0.180	0.0054	0.0024	0.056	0.0003	0.0069	balance
2	12.120	0.113	0.0015	0.182	0.0055	0.0025	0.056	0.0002	0.0056	balance
3	12.250	0.113	0.0015	0.182	0.0053	0.0024	0.057	0.0002	0.0034	balance
EN AC 44100	10.35-13.5	≤ 0.55	≤ 0.10	≤ 0.55	≤ 0.10	≤ 0.10	≤ 0.15	-	-	balance

Figure 1. The cooling curve and the first derivation of the cooling curve recorded at the beginning of casting

Table 3. The characteristic temperatures identified from the obtained cooling curves and its first derivation

T_{Lmax}, °C	T_{Lmin}, °C	T_{Emax}, °C	T_{Emin}, °C	ΔT_L, °C	ΔT_E, °C	T_S, °C	ΔT_{L-S}, °C	Δt_{L-S}, °C
586.57	585.64	526.52	525.9	0.93	0.62	507.43	78.21	32.38

The cooling curve exhibits a typical behavior for Sr modified melts with minimal undercooling and recalescence (Figure 1). The solidification of the melt began by transformation of primary phase at T_{Lmin} of 585.64 °C (Table 3) increasing the liquidus temperature to T_{Lmax} of 586.57 °C. The nucleation of eutectic ($\alpha_{Al}+\beta_{Si}$) phase started at T_{Emin} of 525.90 °C followed by the increase of the eutectic growth temperature to T_{Emax} of 526.52 °C. The nucleation and solidification of the eutectic ($\alpha_{Al}+\beta_{Si}$) phase caused recalescence ΔT_E of 0.62 °C. The solidification sequence lasted for 32.38 s and ended at T_S of 507.43 °C with a cooling rate of 2.42 °C/s. The results of density measurements are indicated in Table 4. The samples solidified on air exhibited higher density values compared to the vacuum solidified samples (Table 4). From the samples solidified on air, the sample 2 had the highest density value of 2.29 gcm^{-3}. Samples 1 and 3 have the same density value of 2.27 gcm^{-3} (Table 4). From the vacuum solidifying samples, the sample 1 exhibits the lowest density value of 2.05 gcm^{-3}. Increasing the melt retention time to 40 min increased the density of the vacuum solidified sample to 2.09 gcm^{-3}

Table 4. The results of melt density measurements

Sample	Density of the sample solidified in air, gcm^{-3}	Density of the sample solidified in vacuum, gcm^{-3}	Gas index, %
1	2.27	2.05	9.63
2	2.29	2.09	8.62
3	2.27	2.16	5.04

(Table 4, sample 2), while melt retention time of 80 min increased density to 2.16 gcm^{-3} (Table 4, sample 3). The highest gas index of 9.63 % was calculated for the sample with retention time of 20 min (Table 4). Increasing the melt retention time to 40 min decreased the gas index to 8.62 %, while the lowest gas index of 5.04 % was calculated for the sample taken at the melt retention time of 80 min.

The radiographs of the samples 1, 2 and 3 with the corresponding cross-sections of the clamp castings are given in Figure 2.
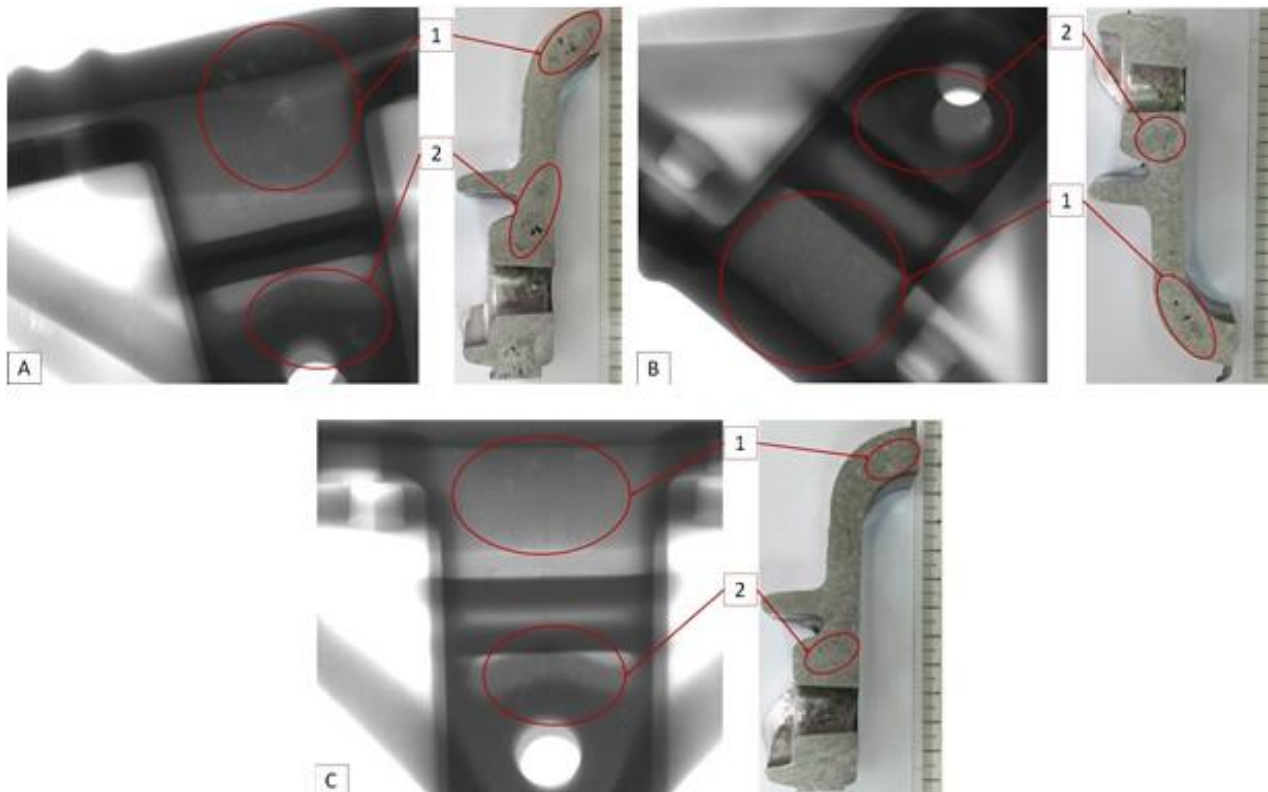

Figure 2. Radiographs and corresponding cross-sections of the samples taken after the melt retention time of: a) 20 min, b) 40 min, c) 80 min.

The results of Radiographic measurements indicate the presence of discontinuities located in the thick sections of the clamp castings (Figure 2, the darkest areas). Based on their morphology the discontinuities can be identified

as porosities (Figure 2). The most prominent properties were obtained in the sample taken 20 min after the Sr addition. The porosities were equally distributed through the thick section of the sample 1 (Figure 2 a). The increase in the melt retention time decreased the severity of porosities (Figure 2 b and c). In the sample with melt retention time of 80 min the porosities can be seen in the last solidifying areas (Figure 2 c). Comparison of the radiographs with the corresponding cross sections of the clamp castings samples indicated the presence of both gas and shrinkage porosities. The gas porosities were most severe in the sample 1 at the positions 1 and 2, and in sample 2 at the position 1 (Figure 2 a and b). The shrinkage porosities were found at the thick sections of the sample 2 (Figure 2 b, position 2) and sample 3 (Figure 2 c, position 2) that are characterized as the last solidifying areas.

The macrostructure and microstructure of the samples 1, 2 and 3 are given in Figure 3.

The macrostructure of sample 1 indicates the presence of shrinkage (Figure 3 a, detail 1) and gas porosities (Figure 3 a, detail 2). In samples 2 (Figure 3 b) and 3 (Figure 3 c) the shrinkage (Figure 3 b detail 1, Figure 3 c detail 1) and gas (Figure 3 b detail 2, Figure 3 c detail 2) porosities are less severe compared to the sample 1. The structure of all three samples consists of primary α_{Al} dendritic network (Figure 3 a, b and c, bright areas) and eutectic ($\alpha_{Al}+\beta_{Si}$) phase (Figure 3 a, b and c, dark areas). In sample 1 the eutectic ($\alpha_{Al}+\beta_{Si}$) phase morphology is fully modified with slightly course eutectic β_{Si} phase particles solidified at the boundaries of eutectic cells (Figure 3 d detail 1). The primary β_{Si} phase particles with polygonal morphology can also be found in the microstructure of the sample 1 (Figure 3 d detail 2). In sample 2 the morphology of eutectic ($\alpha_{Al}+\beta_{Si}$) phase is partially modified (Figure 3 e).
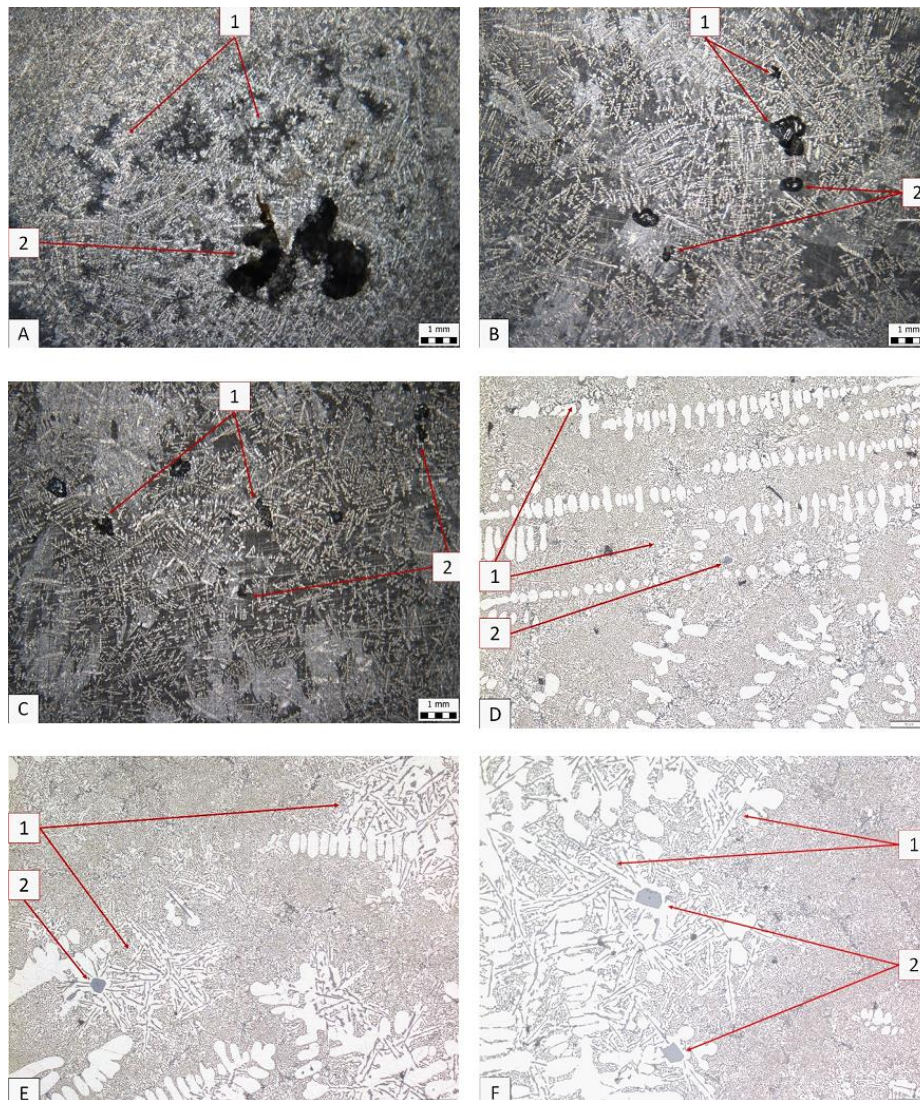

Figure 3. The results of metallographic analysis: a) macrostructure of sample 1, b) macrostructure of sample 2, c) macrostructure of sample 3, d) microstructure of sample 1, e) microstructure of sample 2, f) microstructure of sample 3

The unmodified plate-like eutectic β_{Si} phase particles can be found near the primary α_{Al} dendritic network (Figure 3 e detail 1) and surrounding the primary β_{Si} phase particles (Figure 3 e detail 2). The coarsening of the eutectic β_{Si} phase particles was further enabled by the increase in melt retention time to 80 min (Figure 3 f).

The results of Tensile testing are given in Table 5.

Table 5. The results of melt density measurements

Sample	R_m, MPa
1	133.1
2	93.1
3	87.9

The highest tensile strength of 133.1 MPa was obtained for the samples with the melt retention time of 20 min. Increasing the retention time to 40 min decreased the tensile strength to 93.1 MPa. The lowest tensile strength of 87.9 MPa was measured for the sample 3 obtained after the melt retention time of 80 min.

4. Conclusions

The research was performed to estimate the impact of melt retention time on the Sr modification efficiency. The investigation comprehended determination of chemical composition, density, mechanical properties, and structure investigation of AlSi12 alloy clamp castings taken with retention time of 20 min, 40 min and 80 min. The results of chemical composition analysis indicated the decrease in Sr amount with the prolongation of melt retention time. Despite appropriate addition of AlSr10 master alloy during melt processing, the sufficient amount of Sr required for eutectic (α_{Al}+β_{Si}) phase modification was not achieved. The poor Sr recovery was a consequence of subsequent addition of chemical degassing agents. Their reaction led to the gas entrapment in the melt. Consequently, the highest gas index and most severe porosities were found in sample 1. Prolongation of melt retention time to 40 min and 80 min resulted in the reduction of both gas index and porosities. The fully modified eutectic (α_{Al}+β_{Si}) phase morphology was only obtained in sample 1. After melt retention time of 40 min the unmodified plate-like eutectic β_{Si} phase particles were found. Additional prolongation of melt retention time to 80 min led to the coarsening of eutectic β_{Si} phase particle. In both cases the unmodified plate-like eutectic β_{Si} phase particles were located near the primary α_{Al} dendritic network and surrounding the primary β_{Si} phase particles. This phase distribution suggests that unmodified eutectic β_{Si} phase particles solidify at the beginning of solidification sequence following the transformation of the primary α_{Al} dendritic network.

REFERENCES

[1] Gursoy O., Timelli G., (2020), *Lanthanides: a focused review of eutectic modification in hypoeutectic Al–Si alloys*, Journal of Materials Research and Technology 9, p 8652-8666

[2] Abboud J., Mazumder J., *Developing of nano sized fibrous eutectic silicon in hypereutectic Al–Si alloy by laser remelting*, Scientific Reports 10

[3] Mao F., Qiao Y., Zhang P., Chen C., Zhang C., (2021)., *Modification Mechanism of Rare Earth Eu on Eutectic Si in Hypoeutectic Al-Si Alloy*, International Journal of Metalcasting, 1-12.

[4] Li J. H., Wang X. D., Ludwig T. H., Tsunekawa Y., Arnberg L., Jiang J. Z., Schumacher P., (2015) *Modification of eutectic Si in Al–Si alloys with Eu addition*, Acta Materialia 84, p 153-163

[5] Chankitmunkong S., Eskin D. G., Limmaneevichitr C., (2021), *Effects of Ultrasonic Melt Processing on Microstructure, Mechanical Properties, and Electrical Conductivity of Hypereutectic Al–Si, Al–Fe, and Al–Ni Alloys with Zr Additions*, Light Metals 2021: 50th Anniversary Edition. Springer International Publishing, Oslo, Norway.

[6] Bustos O., Allende R., Leiva R., Sanchez C., (2021), *Effect of magnetic stirring, grain modification and refinement on the solidification structure of an A356 aluminum alloy*, Matéria (Rio de Janeiro) 26.

[7] Yu J., Ren Z., Deng K., (2011), *Refinement and migrating behaviors in Al-Si hypereutectic alloys solidied under electromagnetic vibration*, Acta Metallurgica Sinica 24, p 301-308.

[8] Khan S., Elliott R., (1996), *Quench modification of aluminium-silicon eutectic alloys*, Journal of Materials Science 31, p 3731-3737

[9] Li J. H., Zarif Z. M., Dehm G., Schumacher P., (2014), *Influence of impurity elements on the nucleation and growth of Si in high purity melt-spun Al–Si-based alloys*, Philosophical Magazine 92, No. 31, p 3789-3805.

[10] Cho Y. H., Lee C. H., OH K. H., Dahle A. K., (2008), *Effect of Strontium and Phosphorus on Eutectic Al-Si Nucleation and Formation of β-*

Al₅FeSi in Hypoeutectic Al-Si Foundry Alloys, Metallurgical and Materials Transactions A 39A.

[11] Li, J. H., Barrirero J., Engstler M., Aboulfedl H., Mucklich F., Schumacher P, (2014), *Nucleation and Growth of Eutectic Si in Al-Si Alloys with Na Addition*, Metallurgical And MATERIAls Transactions A 46A, p 1300-1311.

[12] Li J. H., Zarif M. Z., Albu M., McKay B. J., Hofer F., Schumacher P., (2014), *Nucleation kinetics of entrained eutectic Si in Al–5Si alloys*, Acta Materialia 72, p 80-98.

[13] Lu S. Z., Hellawell A., (1987), *The Mechanism of Silicon Modification in Aluminum-Silicon Alloys: Impurity Induced Twinning*, Metallurgical and Materials Transactions A 18A, p 1721-1733.

[14] Hong X., Chen D., Xu Y., Zhu H., Zhang J., Liu Y., Peng Y., Hou L., (2021), *Effect of Different Phosphorus Modifiers on Microstructure and Properties for Al-Si Alloy*, Earth and Environmental Science 692.

[15] Makhouf M. M., Guthy H. V., (2001), *The aluminum–silicon eutectic reaction: mechanisms and crystallography*, Journal of Light Metals 1, p 199-218.

[16] Liao C., Chen J., Li Y., Chen H., Pan C., (2014), *Modification performanceon 4032 Alalloy by using Al–10Sr master alloys manufactured from different processes*, Progress in Natural Science: Materials International 24, p 87-96.

[17] Chen G., Fu G., Yang K., Lin C., (2019) *Study on the Modification Effect of Al-Sr Master Alloy on A356 Aluminum Alloy*, Materials Science Forum 998, p 3-8.

[18] Giovani M., Kaduk J. A., Srirargam P., (2019), Modification of Al-Si Alloys by Ce or Ce with Sr, Jom 71, p 426-434.